Biochimica et Biophysica Acta 1833 (2013) 541–551

Contents lists available at SciVerse ScienceDirect

Biochimica et Biophysica Acta

journal homepage: www.elsevier.com/locate/bbamcr

Anti-mitochondrial therapy in human breast cancer multi-cellular spheroids

Edna Ayerim Mandujano-Tinoco [a,1], Juan Carlos Gallardo-Pérez [a,1], Alvaro Marín-Hernández [a], Rafael Moreno-Sánchez [a], Sara Rodríguez-Enríquez [a,b,*]

[a] Departamento de Bioquímica, Instituto Nacional de Cardiología, México
[b] Departamento de Medicina Translacional, Instituto Nacional de Cancerología, México

ARTICLE INFO

Article history:
Received 24 July 2012
Received in revised form 8 November 2012
Accepted 15 November 2012
Available online 27 November 2012

Keywords:
Breast cancer cell
Glycolysis
Multi-cellular tumor spheroids
Oxidative phosphorylation
Anti-mitochondrial therapy

ABSTRACT

During multi-cellular tumor spheroid growth, oxygen and nutrient gradients develop inducing specific genetic and metabolic changes in the proliferative and quiescent cellular layers. An integral analysis of proteomics, metabolomics, kinetomics and fluxomics revealed that both proliferative- (PRL) and quiescent-enriched (QS) cellular layers of mature breast tumor MCF-7 multi-cellular spheroids maintained similar glycolytic rates (3–5 nmol/min/10^6 cells), correlating with similar GLUT1, GLUT3, PFK-1, and HKII contents, and HK and LDH activities. Enhanced glycolytic fluxes in both cell layer fractions also correlated with higher HIF-1α content, compared to MCF-7 monolayer cultures. On the contrary, the contents of the mitochondrial proteins GA-K, ND1, COXIV, PDH-E1α, 2-OGDH, SDH and F1-ATP synthase (20 times) and the oxidative phosphorylation (OxPhos) flux (2-times) were higher in PRL *vs.* QS. Enhanced mitochondrial metabolism in the PRL layers correlated with an increase in the oncogenes h-Ras and c-Myc, and transcription factors p32 and PGC-1α, which are involved in the OxPhos activation. On the other hand, the lower mitochondrial function in QS was associated with an increase in Beclin, LC3B, Bnip3 and LAMP protein levels, indicating active mitophagy and lysosome biosynthesis processes. Although a substantial increase in glycolysis was developed, OxPhos was the predominant ATP supplier in both QS and PRL layers. Therefore, targeted anti-mitochondrial therapy by using oligomycin (IC_{50} = 11 nM), Casiopeina II-gly (IC_{50} = 40 nM) or Mitoves (IC_{50} = 7 nM) was effective to arrest MCF-7 spheroid growth without apparent effect on normal epithelial breast tissue at similar doses; canonical anti-neoplastic drugs such as cisplatin and tamoxifen were significantly less potent.

1. Introduction

Accelerated glycolysis, even in the presence of saturated O_2 concentration is a common characteristic of all studied neoplasias [reviewed in 1,2]. However, the relevance of oxidative phosphorylation (OxPhos) supporting cancer growth has been documented for a variety of cancer cell lines [1, reviewed in 3] and experimental models, including bi-dimensional [3,4] and tri-dimensional systems (also called human tumor multi-cellular spheroids – MCTS – which resemble early stages of solid tumor) [5–7], and xenografts in mice [8,9]. In this regard, it has been described that OxPhos supports the high ATP demand required during the early stages of HeLa and Hek293 MCTS growth [7]. However, the addition of mitochondrial inhibitors such as Casiopeina-IIgly (CasII-gly) only induces a partial diminution of tumor spheroid growth, indicating that HeLa and Hek293 MCTS proliferation may also be supported by glycolysis [7].

The metabolic reprogramming of mature MCTS (close to 1 mm diameter) involves a marked increase in HIF-1α-activated glycolysis and severe OxPhos depression [7]. The molecular mechanism associated with the glycolytic activation triggered by the development of a hypoxic microenvironment in the tumor core, involves the HIF-1α stabilization and enhancement in the glycolytic gene transcription, protein contents, enzyme activities and flux [reviewed in 10].

Solid tumors develop a tri-dimensional structure that favors the formation of nutrients and oxygen gradients, which in turn promotes the formation of three regions with clearly different phenotypes [11,12]. These three well-defined regions (the proliferative, quiescent and the necrotic center) have been analyzed as a whole, *i.e.*, in mature, entire MCTS (HeLa, Hek293, U343MG, EMT6/Ro, BT474, DU145, T47-D) in which growth rate, morphology and physiology have been determined [7,13–21]. However, the phenotypic characteristics determined in

Abbreviations: Atg7, autophagy-related gene 7; Bnip 3, Bcl2/adenovirus EIB 19 kD-interacting protein 3; COXIV, cytochrome oxidase subunit IV; GA-K, glutaminase-K; GLUT, glucose transporters; HK, hexokinase; HIF-1α, hypoxia inducible factor-1 alpha; LAMP, lysosome-associated membrane proteins; LDH, lactate dehydrogenase; LC3B, autophagy marker light chain 3 isoform B; MCT-1, monocarboxylate transporter-1; MCTS, multi-cellular tumor spheroids; ND1, NADH dehydrogenase (complex I) subunit 1; PDH, pyruvate dehydrogenase; PGC-1α, peroxisome proliferator activated receptor gamma coactivator-1 alpha; PRL, proliferative cell layers of tumor spheroids; QS, quiescent cell layers of tumor spheroids; SDH, succinate dehydrogenase; 2OG, 2-oxoglutarate; 2OGDH, 2-oxoglutarate dehydrogenase

* Corresponding author at: Departamento de Bioquímica, Instituto Nacional de Cardiología, Juan Badiano No. 1, Col. Sección 16, Tlalpan, México D.F. 14080, México. Tel.: +52 55 55 73 29 11x1422.
E-mail address: saren960104@hotmail.com (S. Rodríguez-Enríquez).

[1] Edna A. Mandujano-Tinoco and Juan C. Gallardo-Pérez equally contributed to the experimental work of this paper.

0167-4889/$ – see front matter © 2012 Elsevier B.V. All rights reserved.
http://dx.doi.org/10.1016/j.bbamcr.2012.11.013

whole spheroids may not reflect the intrinsic signature of each region inside the tumor derived from the large metabolite and oxygen fluctuations throughout the spheroid [11,21].

Regarding energy metabolism, scarce information is available on its cellular zonation across MCTSs. Freyer [16,22] described a severe diminution in the rhodamine123 retention, and presumably oxygen consumption, in both outer and inner cellular layers of EMT6 mouse mammary carcinoma and 9L rat glioma MCTSs in comparison to cells grown as monolayers [16,22]. Unfortunately, the rhodamine123 concentration used in these studies promotes severe perturbation to the OxPhos by acting both as an uncoupler and an inhibitor of the ATP/ADP translocator and ATP synthase [23,24], making difficult the interpretation of results. In addition, the cellular oxygen consumption measurements in MCTSs have not usually been corrected by using a respiratory chain inhibitor or oligomycin to discard the O_2-uptake by non-mitochondrial enzymes, whose activity is 2.5–5 times increased in tri-dimensional models [25,26].

In solid tumors and probably in MCTS models, prolonged hypoxia promotes a metabolic symbiosis in which the lactate overproduced by the highly glycolytic and hypoxic cells (*i.e.*, inner, and presumably, quiescent cell layers) is actively consumed by the blood-closer and well-oxygenated cells (*i.e.*, external layers) for oxidative metabolism. This metabolic switch involves the over-expression of, at least, two proteins in the oxidative tumor cells, which are required for the massive lactate uptake (MCT-1) and for the rapid cytosolic lactate oxidation (LDH-B) to generate pyruvate, which in turn, enters into the mitochondria for generation of reducing equivalents and ATP [27]. These observations strongly suggest that the micro-area, in which the tumor cell lies inside MCTS, may modify the energy cellular metabolism. Therefore, the identification of the principal energy supply pathway for each cellular population in the MCTSs, and solid tumors, and hence the use of specific and potent metabolic inhibitors against this particular pathway may be considered as a potential anti-tumor strategy.

To analyze the bioenergetics of the MCTS external and inner cellular layers, proteomic analysis, kinetic determinations and metabolic fluxes of OxPhos and glycolysis were performed in disaggregated mature spheroids. In parallel, the expression patterns of several transcription factors involved in the modulation of glycolysis and mitochondrial metabolism were also analyzed. Once the principal ATP producer was identified, specific anti-tumor therapy was designed for the entire mature MCTS using permeable and selective inhibitors to diminish tumor growth. In parallel, canonical chemotherapy drugs were evaluated on MCTS growth for comparative purposes. Results of the present study may contribute to the better understanding of the energy metabolism changes in the basic unit of tumor growth and provide guidance in the design of more appropriated targeted clinical treatment strategies.

2. Materials and methods

2.1. Monolayer and spheroid cultures

Breast human tumor stage-3 MCF-7 (1×10^7 cells/dish) and the normal epithelial breast MCF-12A cells (American Type Culture Collection; Rockville, MD, USA) were grown in Dulbecco-MEM medium supplemented with 10% fetal bovine serum (GIBCO; Rockville, MD, USA) plus 10,000 U penicillin/streptomycin (SIGMA; Steinheim, Germany) and placed under a humidified atmosphere of 5% CO_2/95% air at 37 °C during 3–4 days until confluence of 80–90% was reached. The genotyping of the MCF-7 cells (National Institute of Genomic Medicine, Mexico) used in the present study revealed that they are already a subclone because they only share 5 out of 14 canonic allelic markers with the original MCF-7 clone (American Type Culture Collection; Rockville, MD, USA). Afterwards, cells were gently detached from the culture dish by a 2–3-min exposure to 3 mL of 0.25% trypsin/EDTA (GIBCO), followed by washing with fresh Krebs–Ringer medium (125 mM NaCl, 5 mM KCl, 1 mM $MgCl_2$, 1.4 mM $CaCl_2$, 1 mM H_2PO_4, 25 mM HEPES, pH 7.4) and centrifugation at $300\times g$ for 2–4 min at room temperature [28].

MCF-7 and MCF-12A spheroids were formed by using the liquid overlay modified technique [29,30]. Briefly, 1×10^5 cells were seeded in 2% (w/v) agarose-coated Petri dishes. Once spheroids reached a diameter of 100 ± 57 (MCF-7; $n=140$) or 197 ± 30 (MCF-12A; $n=80$) μm, medium was replaced with fresh medium and placed under slow (20–50 rpm) orbital shaking for additional 14–18 (MCF-7) or 9–10 (MCF-12A) days at 37 °C under 95% air/5% CO_2. Fresh medium was added every 2–3 days to remove cellular debris and non-well formed spheroids. The size of breast tumor and non-tumor spheroids was measured at different culture times with a graduated reticule (1/10 mm; Zeiss, Thornwood, NY, USA) in an inverted phase contrast microscope (Zeiss).

2.2. Selective disaggregation of MCF-7 spheroids

Mature spheroids (863 ± 64 μm diameter after 20 days of culture; $n=140$; Fig. 1A) were sequentially trypsinized using the standard dissociation method [13] to separate both external (proliferative) and internal (quiescent + apoptotic) cell populations. Briefly, 20–40 spheroids were exposed to 5 mL 0.25% trypsin/EDTA under gentle orbital agitation (20–50 rpm) at 37 °C for 3 min. Then, two fractions were collected: a supernatant containing proliferative cells and a bottom constituted by the quiescent cells. Both cellular fractions were gently washed with fresh medium and centrifuged at $34{,}000\times g$ for 5 min, at 37 °C. The cellular bottoms were re-suspended in fresh D-MEM and stored at room temperature until use. Cellular viability was determined by using the blue trypan method [4], which yielded values of 87 ± 8 and $>95\pm5\%$ for quiescent (QS) and proliferative (PRL) cell-enriched layers, respectively. Cellular protein was determined by using the Biuret assay as described elsewhere [4].

To determine the growth capacity of each isolated MCTS (QS or PRL) fraction, the cells (5×10^4 cells) were seeded in 1 mL D-MEM in 24 multi-well plates and incubated at 37 °C, under 5%CO_2/95% air. Cellular numbers were quantified every 48 h until 144 h of culture by using the trypan blue assay [4].

2.3. Immunohistochemical analyses of the MCTS

Mature spheroids were fixed by incubating with 10% paraformaldehyde at 4 °C overnight and washed with fresh phosphate buffer. Afterwards, spheroids were embedded in paraffin and sectioned into 2 μm thick layers. Cut layers were stained with the primary Ki-67 antibody (Santa Cruz, CA, USA) at a final dilution of 1:70 for 20 min or with hematoxylin & eosin (H&E). The Ki67 and H&E detection was performed in the automated BenchMark ULTRA system (Roche, Tucson, AZ, USA) using the ultraView Universal DAB detection system (Ventana Medical System Inc, Tucson, AZ, USA) following established protocols [31].

2.4. Determination of metabolic fluxes

For OxPhos flux, oligomycin-sensitive respiration was determined at 37 °C in both quiescent ($3.5–4\times10^6$ cells) and proliferative ($1–1.5\times10^6$ cells) cell fractions by using a Clark-type electrode in an air-saturated Krebs–Ringer medium plus 5 mM glucose. To reveal the activity of the respiratory chain, KCN-sensitive respiration was also determined. For glycolysis, both outer (proliferating) and inner (quiescent) cell-enriched layers ($1–30\times10^6$ cells) were pre-incubated for 10 min in 3 mL Krebs–Ringer medium under orbital shaking (150 rpm, 37 °C) and afterwards, 5 mM glucose was added. After 3 min, samples were precipitated with 3% (v/v) ice-cold perchloric acid and neutralized with 3 M KOH/0.1 M Tris. Neutralized samples were used for lactate, ATP and ADP determinations [32]. L-Lactate generated by glycolysis was determined by using lactate dehydrogenase following the NADH formation at 340 nm [33].

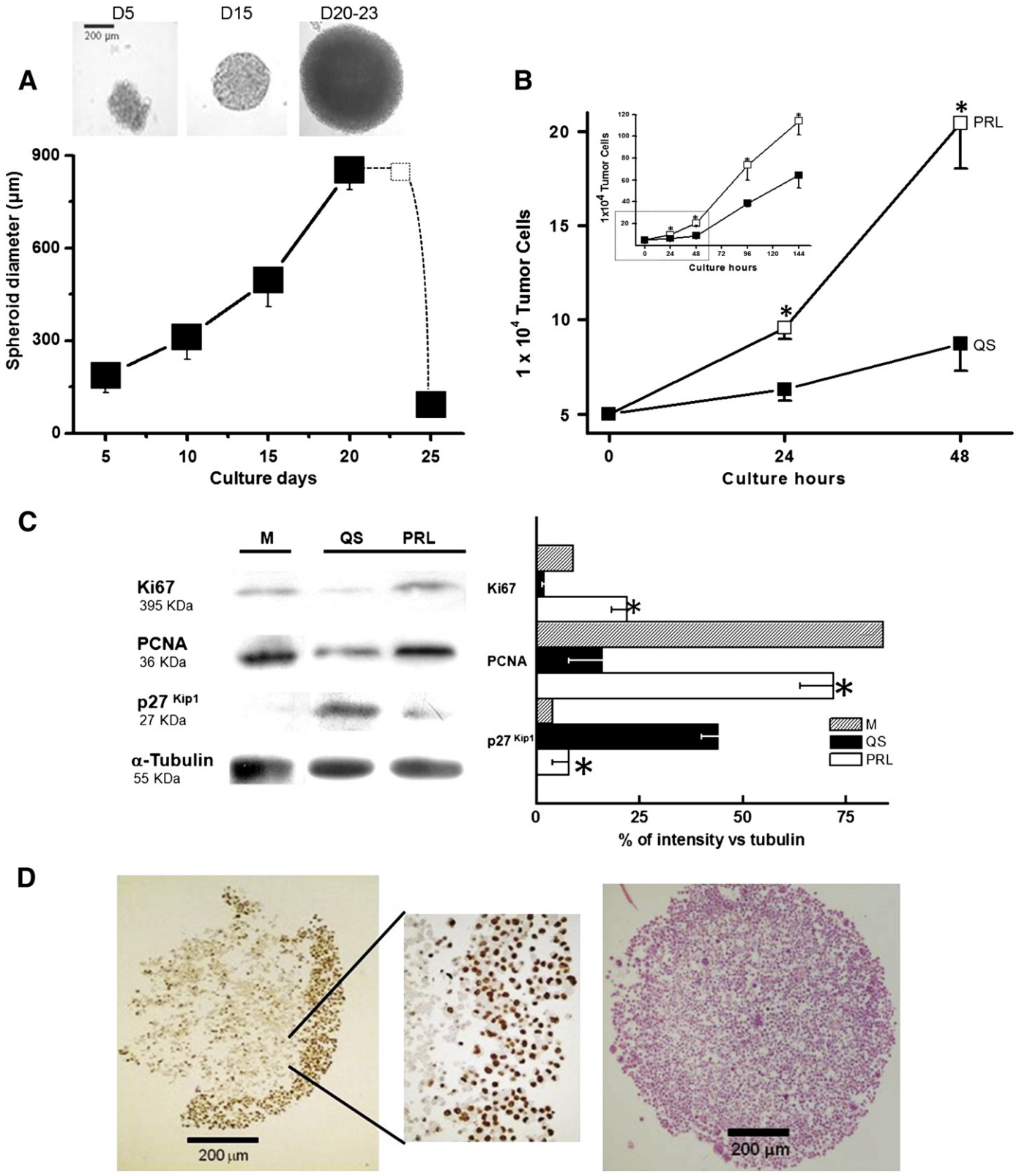

Fig. 1. (A) MCF-7 spheroid growth and MCTS cell layer proliferative profile. Diameters of at least 70 MCF-7 spheroids were determined from day 5 to day 20. At day 24 or 25, massive cellular disintegration was detected. Upper panel insert shows a micrography of the 5, 15 and 20–23 day (D) old MCF-7 MCTSs; bar represents 200 µm. (B) Proliferative (PRL) and QS (quiescent) layers coming from disaggregated MCF-7 spheroids were cultured in monolayer as described under Materials and methods. *$P<0.05$ *vs.* QS, $n=3$, for non-paired two-tailed Student's *t* test and one way ANOVA. (C) Proteomic analysis of PRL and QS markers in MCF-7 QS and PRL cells. Bars represent the mean ± SD of 75 spheroids. *$P<0.05$ *vs.* QS. (D) Representative immunohistochemistry images of 14 Ki67-stained (left panel; $n=14$) or 8 hematoxylin & eosin-stained (right panel; $n=8$) mature MCF-7 spheroids. Due to the fragility of the samples no always manageable cuts from entire spheroids were attained.

2.5. Determination of enzyme activities

For cytochrome *c* oxidase (COX) determination, cells were incubated in air-saturated KME (125 mM KCl, 20 mM MOPS and 1 mM EGTA, pH 7.4) buffer plus 0.02% Triton X-100, 50 μM horse muscle cytochrome *c* and 5 mM sodium ascorbate at 37 °C. The oxidation of reduced cytochrome *c* was spectrophotometrically monitored at 550 minus 540 nm in a dual-beam UV-visible spectrophotometer (2501PC, Shimadzu, Japan). The COX reaction was started by adding 1 mg cellular protein/mL. In parallel experiments, 20 mM sodium azide or 1 mM KCN was added to specifically block COX activity [34]. Succinate dehydrogenase (SDH) activity was assayed in SHE (250 mM Sucrose, 10 mM HEPES and 1 mM EGTA, pH 7.3) buffer plus 0.5 mg cellular protein/mL, 0.2 mM 2,6-dichloroindophenol (DCPIP), 0.4 mM phenazine methosulfate (PMS), 0.02% Triton X-100, 50 μM $MgCl_2$ and 1 mM cyanide at 37 °C. The reaction was started by adding 10 mM succinate and the rate of DCPIP reduction was determined by measuring the absorbance change at 600 nm using an extinction coefficient of 21.3 mM^{-1} cm^{-1} [35].

For glycolytic enzyme activities, cellular extracts from both proliferating and quiescent cells (30×10^6 cells or 2 mg cellular protein/mL) were suspended in 25 mM Tris–HCl buffer, pH 7.6 plus 1 mM EDTA, 5 mM DTT and 1 mM PMSF, and subjected to three cycles of freezing in liquid N_2 and thawing at 37 °C [36]. Hexokinase (HK) activity was assayed in 50 mM MOPS buffer, pH 7.0 at 37 °C in the presence of 2 U glucose-6-phosphate dehydrogenase (Roche; IN, USA), 1 mM $NADP^+$, 15 mM $MgCl_2$, 10 mM ATP and 20–60 μg cellular extract protein/mL. The reaction was started by adding 3 mM glucose after 3 min of pre-incubation and generation of NADPH was measured at 340 nm. The activity of hexosephosphate-isomerase (HPI) was determined in 50 mM MOPS buffer, pH 7.0 at 37 °C plus 2 U glucose-6-phosphate dehydrogenase, 1 mM $NADP^+$ and 10–20 μg cellular extract protein/mL. The reaction was started by adding 2 mM fructose-6-phosphate. Lactate dehydrogenase (LDH) was assayed in 50 mM MOPS, pH 7.0 at 37 °C, 0.15 mM NADH and 10–20 μg cellular extract protein/mL; after 3 min pre-incubation, the reaction was started with 1 mM pyruvate and NAD^+ formation was registered at 340 nm. All enzymatic assays showed no reaction when the specific substrates were omitted [36].

2.6. Proteomic analysis

For Western blot, quiescent and proliferative cells were dissolved in RIPA (PBS 1× pH 7.2, 1% IGEPAL NP40, SDS 25% and sodium deoxycholate 0.05%) lysis buffer plus 5 mM of protease inhibitors (Roche, Mannheim, Germany). Protein (40 μg) was re-suspended again in loading buffer plus 5% β-mercaptoethanol and loaded onto 12.5% polyacrylamide gel under denaturalizing conditions [7]. Electrophoretic transfer to PVDF membranes (BioRad; Hercules, CA, USA) was followed by overnight immunoblotting with 1:1000 dilution of PCNA, $p27^{Kip1}$, α-tubulin, GLUT-1, GLUT-3, HKII, LDH-A, α-KGD, GA, ANT, ND1, COX-IV, PDH-E1α, SDHC, p32, p53, TIGAR, PGC-1α, H-Ras, c-Myc, Atg7, Beclin, LC3B, and LAMP-1 antibodies; or 1:200 dilution of PFK-1, GAPDH, ATP synthase, Bnip3 antibodies; or 1:500 dilution of Ki-67 antibody; or 1: 5000 dilution of HIF-1α antibody at 4 °C. All antibodies were purchased from Santa Cruz Biotechnology (Santa Cruz, CA, USA). The hybridization bands were revealed with the corresponding secondary antibodies conjugated with peroxidase (Santa Cruz). The signal was detected by chemiluminescence using the ECL-Plus detection system (Amersham Bioscience; Piscataway, NJ, USA). Densitometric analysis was performed using the Scion Image Software (Scion Corp, Bethesda MD, USA) and normalized against its respective load control. Percentage of each isoform represents the mean ± SD of at least three independent experiments.

2.7. Proteomic analysis of transcription factors and oncogenes in bi-dimensional MCF-7 cultures under chronic hypoxia

MCF-7 monolayer cultures at 80–90% confluence were placed in a humidified hypoxia incubator chamber (Billups-Rothenberg; Del Mar, California, USA) saturated with 95% N_2/5% CO_2 to give approximately 0.1% $O_{2atmospheric}$ at 2240 m altitude and further incubated at 37 °C for 24 h. Afterwards, cells were collected and processed as described in the Proteomic analysis section.

2.8. Half maximal inhibitory concentrations (IC_{50}) for mitochondrial and glycolytic inhibitors and for canonical anticancer-drugs on growth of normal epithelial breast and tumor breast spheroids

Both MCF-7 and MCF-12A spheroids were cultured in DMEM and in the presence of glycolysis (iodoacetate) or OxPhos (rhodamines 123 and 6G, Casiopeina II-gly, oligomycin, Mitoves) inhibitors or in the presence of the canonical anti-tumor drugs tamoxifen or cisplatin. Inhibitors were sterilized by filtration and added at the beginning of MCTS formation (day 5 for both spheroids, once the primary core was formed). The DMEM medium plus the inhibitor was replaced every three days. The IC_{50} values were determined at day 17 (MCF-7) or at day 11 (MCF-12A). In a second set of experiments, the drugs were added to mature tumor spheroids (at day 15 of culture, diameter ≈500 μm) and the medium plus inhibitor was replaced every three days. Mitoves, oligomycin, tamoxifen and cisplatin were diluted in 70% ethanol/30%DMSO. The addition of vehicle did not modify the MCTS growth.

2.9. Statistical evaluation

Data are expressed as mean ± SD of the indicated number of independent experiments. Analysis was performed using non-paired two-tailed Student's *t* test; P values less than 0.05 were considered significant.

3. Results

3.1. Cellular growth and specific markers of proliferative and quiescent MCF-7 spheroid layers

In order to assess the proliferative capacity of each MCF-7 spheroid cell population, cellular growth as well as the expression of the proteins p27 (a selective quiescence marker whose expression is associated with the inhibition of cyclin E/A-cdk2 complex), and Ki67 and PCNA (selective proliferation markers whose expression is associated with the activation of the cellular cycle) [37,38] were determined in both the outer proliferative (PRL) and inner quiescent (QS) enriched cellular fractions. After 48 h incubation (Fig. 1B), the cellular number of the PRL fraction was significantly higher (from 5×10^4 to $20\pm10\times10^4$ cells) than that attained by the QS fraction (from 5×10^4 to $8\pm1\times10^4$ cells; $P<0.005$). At the 24 and 48 h-point (Fig. 1B), the number of generations of the QS fraction was significantly lower (0.3 ± 0.08 and 0.4 ± 0.1 generations/24 h, respectively) compared to that attained by the PRL fraction (0.9 ± 0.1 and 1 ± 0.07 generations/24 h); these last values were close to the value calculated for the proliferation of MCF-7 cells in monolayer (1 ± 0.2 generations/24 h) [28]. Interestingly, after 48 h culture the QS fraction proliferative capacity was similar to that determined for the PRL layer (1.1 ± 0.1 *vs.* 0.9 ± 0.05 generations/24 h, respectively); however, the final cellular content after 144 h was significantly lower in the QS fraction than in the PRL fraction (insert Fig. 1B).

The higher proliferation rate of the PRL cell fractions correlated with their PCNA (3.4-fold) and Ki67 (5-fold) higher contents, and p27 lower content (4.5-fold) *versus* the QS cell fractions (Fig. 1C). As a comparative model, MCF-7 monolayer cultures were also analyzed.

The PCNA, p27 and Ki67 contents observed for the MCTS PRL fraction were similar to those observed for monolayer culture cells (Fig. 1C), which demonstrated the proliferative status of the spheroid PRL cell layer. To further support the proliferative phenotype of the PRL cell fraction, the Ki67 content was also analyzed by immunohistochemistry in the entire fixed mature MCF-7 MCTS (Fig. 1D, left panel). Dark spots in the periphery of the spheroid represent the high Ki-67 intensity observed in PRL layer confirming their proliferative phenotype. On the other hand, clear spots were observed in the inner MCTS cell layer indicating scarce Ki67 staining which confirms their quiescent phenotype. Hematoxylin & eosin stain in the MCF-7 entire mature spheroid revealed high cellular viability in both QS and PRL layers and the complete absence of a necrotic center (Fig. 1D, right panel). Therefore, the whole set of results shown in Fig. 1 clearly shows the presence of two viable cell populations in mature MCTS with different proliferative capacities.

3.2. Proteomic, kinetomic and fluxomic analyses of glycolysis and OxPhos in the MCF-7 MCTS proliferative and quiescent cells

High glycolytic capacity coupled to an enhanced HIF-1α level is an important metabolic characteristic of solid tumors [39–41]. In both MCTS quiescent and proliferative enriched cell fractions, HIF-1α protein was significantly higher (1.8–3.1-times) in comparison with normoxic monolayer cultures (Fig. 2A). In consequence, as most of the glycolytic proteins are up-regulated by HIF-1α [10], an increased glycolytic flux was determined for both cell layers (Table 1), which was higher compared to that found in MCF-7 monolayer cultures, rat hepatocytes, and tumor normoxic bi-dimensional cultures (MDA-MB-453, HeLa, Hek293) and even in tumor cells exposed to prolonged hypoxia in monolayer cultures [28,36,42].

Increased glycolytic flux in both MCTS QS and PRL cells correlated with high contents (245–544% *vs.* tubulin) and activities of flux-controlling (HK, GLUT1) and non-controlling (HPI, LDH) glycolytic enzymes and transporters [36] (Fig. 2A, Table 1). This high expression pattern was not observed for other glycolytic proteins such as GLUT3, PFK-1 and GAPDH. The contents of GLUT1, HKII and LDH-A in both MCTS cell fractions were also significantly higher than those found in normoxic MCF-7 monolayer cultures (Fig. 2A). On the other hand, the activities of HK and LDH (Table 1) in both QS and PRL fractions were higher than those reported for normal tissue [43–45] and within the same range determined for bi-dimensional MCF-7 cultures (10 ± 6, $n = 3$ and 100, $n = 2$ mU/mg protein, respectively) and entire MCTSs [28].

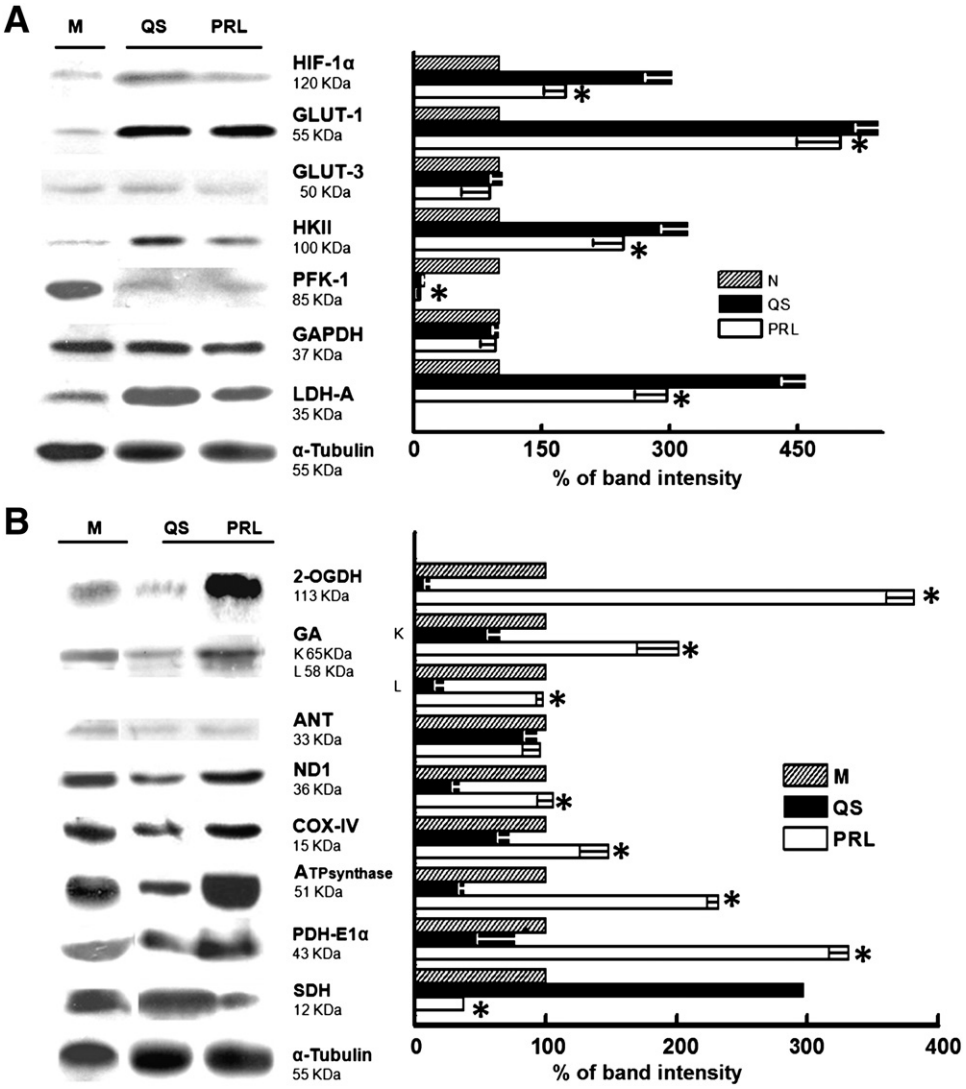

Fig. 2. Proteomic analysis of (A) HIF-1α and glycolytic proteins in MCF-7 monolayer (M), MCF-7 MCTS quiescent (QS) and proliferative (PRL) cells. Data represent mean ± SD of 50 spheroids. *$P \leq 0.05$ *vs.* QS. (B) Mitochondrial proteins in MCF-7 monolayer (M), MCF-7 MCTS quiescent (QS) and proliferative (PRL) cells. Data represent mean ± SD of 50 spheroids. *$P \leq 0.05$ *vs.* QS.

Table 1
OxPhos and glycolysis in monolayer MCF-7, quiescent (QS) and proliferative (PRL) MCF-7 MCTS cellular populations.

	Monolayer	% ATP produced	QS	% ATP produced	PRL	% ATP produced
Total respiration	9.4 (2)		62 ± 20 (7)*		113 ± 28 (6)	
OxPhos	6.7 (2)	92	25 ± 10 (7)*	93	53 ± 18 (6)	**98**
SDH	3.3 ± 1.2 (4)*		2.3 ± 1.3 (4)*		5.2 ± 1.9 (4)	
COX	ND		1 ± 1 (4)		3 ± 2 (4)	
Glycolysis	1.4 ± 0.8 (4)*	8	4.5 ± 2 (3)	**7**	3.1 ± 1.6 (3)	**2**
HK	7.7 ± 4.6 (3)		11 ± 8 (5)		14 ± 4 (4)	
HPI	736 ± 228 (3)		579 ± 282 (5)		669 ± 333 (4)	
LDH	100 (2)		393 ± 133 (5)		566 ± 330 (5)	
ATP	9.2 ± 2.3 (3)		8 ± 1 (3)		9 ± 3 (3)	
ADP	1.6 ± 0.4 (3)		1.3 ± 0.5 (3)		2.1 ± 0.5 (3)	

Fluxes are expressed in ngAO/min/10^6 cells for OxPhos and in nmol/min/10^6 cells for glycolysis. KCN-sensitive respiration was 52 ± 24% and 73 ± 11% of total respiration ($n = 4$) for QS and PRL cells, respectively. Activities are expressed in mU/10^6 cells. Nucleotides are expressed in nmol/10^6 cells. OxPhos ATP-contribution was calculated assuming a P/O ratio of 2.5 [88], whereas for glycolysis, 1 ATP = 1 lactate. Data represents mean ± SD. (n) represents the number of different spheroid preparations analyzed. *$P < 0.05$ *vs.* PRL. Abbreviations: COX, cytochrome *c* oxidase; HK, hexokinase; HPI, hexose-phosphate isomerase; LDH, lactate dehydrogenase; SDH, succinate dehydrogenase. The viability of the cells was >85% for both PRL and QS layers.

Cells derived from the MCTS proliferating layers showed 2-times higher total oxygen consumption and oligomycin-sensitive respiration (OxPhos) than cells derived from the MCTS quiescent layer (Table 1). In turn, both QS and PRL layers OxPhos fluxes were 3–7 times higher than that determined for the normoxic MCF-7 monolayer cells (Table 1) and for the entire MCTS [7,28]. Increased total cellular respiration and OxPhos in proliferative cells correlated with a significant elevation in the contents of the mitochondrial enzymes 2-OGDH (34-times), PDH-E1α subunit (4.4-fold), glutaminase-K (3-times), respiratory chain NADH dehydrogenase complex 1 (3.1-fold) and cytochrome *c* oxidase complex IV (2-times); and ATP synthase subunit 5 (6-times) (Fig. 2B), compared to QS cells. Activities of COX and SDH (3-times) also increased in MCTS proliferative cell layer *vs.* MCTS quiescent cells (Table 1). The protein contents of ND1 and ANT found in the PRL layers were similar to those observed in normoxic monolayer cultures; however, the contents of other mitochondrial proteins such as 2-OGDH, GA-K, PDH-E1α and ATP synthase were significantly higher, or lower (SDH), in PRL compared to bi-dimensional cultures (Fig. 2B).

Although high glycolytic rates were determined in both MCTS proliferative and quiescent cell layers, contribution to ATP supply by glycolysis was less than 10%, indicating that MCTS, like MCF-7 monolayer cells (Table 1), strongly depend on OxPhos [28]. On the other hand, steady state ATP and ADP concentrations, as well as the ATP/ADP ratio were similar in both MCTS quiescent and proliferative cells as well as MCF-7 bi-dimensional culture (Table 1) [28].

3.3. Expression of autophagic proteins and transcription factors associated with changes in mitochondrial metabolism in quiescent and proliferative layers

In an initial attempt to determine the mechanisms associated with the high OxPhos flux and mitochondrial protein contents in the PRL cells, the pattern of transcription factors involved in the regulation of tumor mitochondrial metabolism [46,47] was evaluated in both MCTS cellular fractions and compared to monolayer cells exposed to normoxic and hypoxic conditions (Fig. 3A). In the PRL layers where OxPhos predominates for ATP-supply (Table 1), the main transcription factors involved in the *de novo* synthesis of respiratory chain components (p32 and h-Ras), β-oxidation (PGC-1α) [reviewed in 48] and mitochondrial biogenesis (c-Myc) [46,47,49] significantly increased (53–73%) *versus* the quiescent cell layers (Fig. 3A). The protein contents of p32, p53, c-Myc and h-Ras in the PRL layers were similar to those found in normoxic-MCF7 monolayer cells, whereas the PGC-1α level was remarkably higher in the PRL layers. On the other hand, p32 and h-Ras levels found in QS layers were significantly lower to those observed in hypoxic MCF-7 monolayer cells, suggesting that hypoxia is not the only factor that modulates expression of these transcription factors inside the tumor spheroids (Fig. 3A).

Interestingly, diminution in OxPhos flux, and COX and SDH activities in QS cells (Fig. 2B, Table 1) correlated with high contents of p53 (Fig. 3A) and autophagy proteins (Beclin, LC3B, Bnip3 and LAMP) compared with PRL cells, indicating mitophagy activation (Fig. 3B). TIGAR, a glycolytic tumor modulator was expressed at similar levels in both MCTS layers correlating with similar glycolytic enzyme activities, transporter and enzyme contents, and flux rates (Table 1). As the oxygen concentration in the inner QS layers of mature MCTS is low (7–14 μM O_2, [11]), and to make a stricter comparison, the contents of the mitophagy proteins were also analyzed in MCF-7 monolayer cultures exposed to prolonged and chronic hypoxia (24 h, 13 μM O_2 [28]). The levels of p53, TIGAR, and autophagy proteins, except for Atg7, in the QS layers were similar to the protein profiles determined in the MCF-7 monolayer model exposed to chronic hypoxia (Fig. 3B).

3.4. Sensitivity of MCTS growth to energy metabolism inhibitors and canonical anticancer drugs

The results shown in the previous sections clearly demonstrated that the well-formed QS and PRL cellular layers constituting the entire MCF-7 spheroid depend on OxPhos for ATP supply (Table 1). This finding may presumably also be applied to the growth of solid tumors. Therefore, the addition of typical mitochondrial inhibitors but not glycolytic inhibitors should induce a severe arrest of the MCF-7 MCTS growth. To assess this hypothesis, MCF-7 spheroids were cultured in the presence of oligomycin (a specific mitochondrial ATP synthase inhibitor) or iodoacetate (IAA, a GAPDH inhibitor) [50; reviewed by 51] (Fig. 4A). Oligomycin abolished the growth of MCF-7 at remarkably low concentrations whereas no apparent effect was achieved by IAA (Table 2). However, oligomycin is also extremely toxic for normal, healthy cells [52,53].

Then, rhodamines 123 (rhod123) and 6G (rhod6G), Casiopeina II-gly (CasII-gly) and Mitoves (MV11), lipophilic cationic drugs with potent inhibitory effect on mitochondrial metabolism, and the canonical anticancer drugs tamoxifen and cisplatin [reviewed by 51, 54] were also evaluated for their effects on MCTS growth (Fig. 4A). For a rigorous comparative analysis, CasII-gly, MV11 and cisplatin (CP) were also assayed in non-tumor but highly proliferative normal breast cell line MCF-12A. CasII-gly and MV11 severely abolished the growth of MCTSs at therapeutically relevant low doses (Table 2) whereas rhodamines 123 and 6G were less effective. Compared to the canonical chemotherapy drugs tamoxifen (Tam) and CP, CasII-gly and MV11 showed higher potency against MCTS cells. Remarkably, these energy metabolism drugs were approximately one order of magnitude more selective for

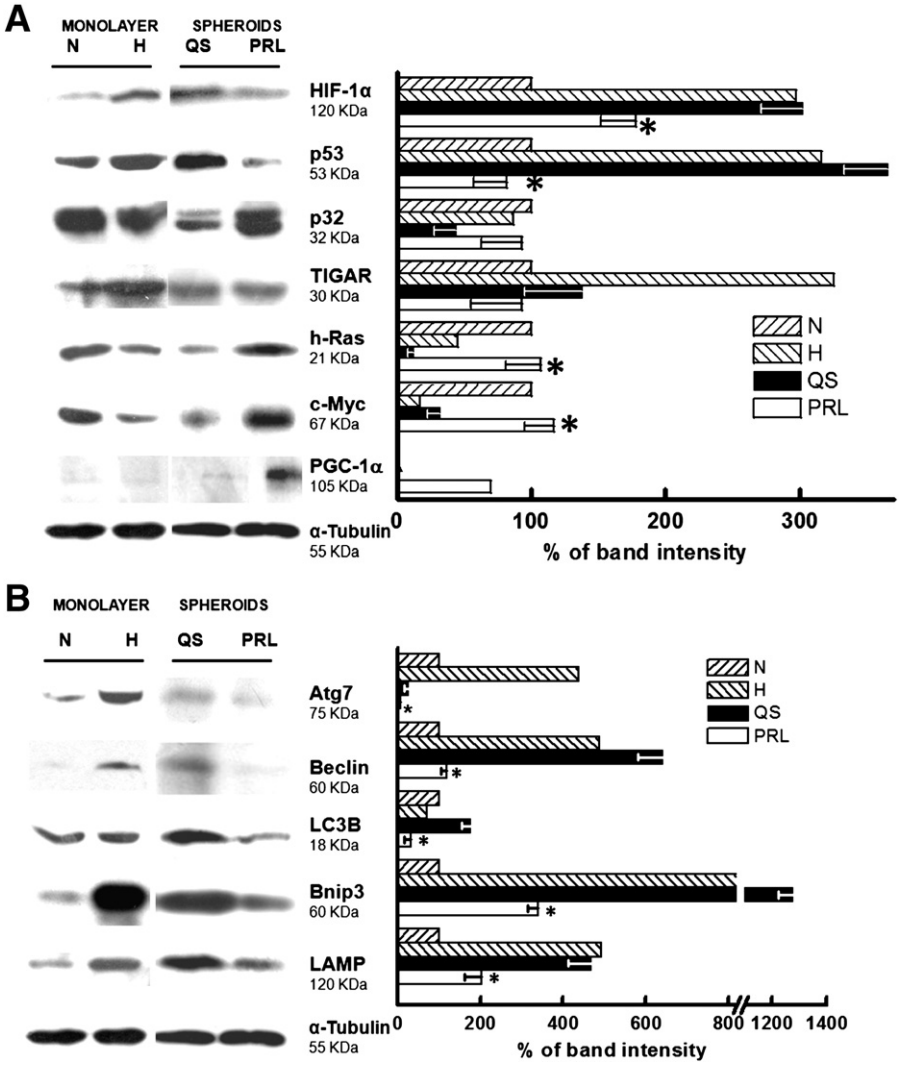

Fig. 3. Proteomic analyses of (A) transcription factors and (B) mitophagy proteins involved in the regulation of the mitochondrial function in QS and PRL cells from MCF-7 MCTSs. As a control, the proteomic analysis was also carried out with monolayer MCF-7 cells exposed to normoxic (N, 21% O_2) or hypoxic (H, 0.1% O_2) conditions for 24 h. Data represent mean ± SD of 50 spheroids. *$P \leq 0.05$ *vs.* QS.

MCTS than for normal breast spheroids, whereas CP showed similar potencies for both types of spheroids (Table 2, Fig. 4B).

Well-formed MCTSs of 500 μm diameter (day 15) were also exposed to CasII-gly, MV11 or CP. After three days, MV11 completely arrested growth, whereas Cas-IIgly and CP were relatively innocuous (Fig. 5A). However, six days later (day 21), CasII-gly and CP also abolished growth and induced cell death (Table 2, Fig. 5B).

4. Discussion

Bi-dimensional cultures of cancer cells have been profusely employed as a model for analyses of their radio- and chemotherapy response, intermediary metabolism, bioenergetics studies, and signaling [36,55,56] among others, providing useful information for understanding tumor physiology. However, the monolayer cultured tumor cells do not strictly reflect the behavior of solid tumors regarding the spatial organization. Three-dimensional multi-cellular tumor spheroids (MCTSs) better resemble the heterogeneous microenvironment found in solid tumors, in which physiological and biochemical differences throughout the cellular layers are generated [57]. Therefore, strategies directed to slow-down the accelerated tumor cell proliferation should take these spatial-driven changes into account to be able to improve treatment protocols. In the present study we characterized the predominant energy metabolism in each cellular layer derived from an early-stage solid tumor model to propose alternative therapies for cancer treatment improvement.

4.1. Enhanced OxPhos in MCTS proliferative-enriched cell fractions, and depressed OxPhos in quiescent-enriched cell fractions

After disaggregation of mature MCTSs, the two separated cellular layers showed different proliferation profiles (*cf.* Fig. 1), indicating that indeed, QS and PRL-enriched cell fractions contain distinctive cellular subpopulations with contrasting metabolic changes. In terms of energy metabolism, glycolysis and OxPhos have been analyzed in whole MCTSs (HeLa, Hek-293, transformed rat embryo fibroblasts, BMG-1, HepG2) where glycolytic metabolism seems to be the principal cellular ATP supply [7,58–60]. However, prolonged anti-glycolytic treatments in the entire MCTSs do not block tumor proliferation, suggesting that OxPhos has also a significant role in sustaining cellular growth [7,59].

No information is yet available regarding analysis of both OxPhos and glycolysis in dissected tumor spheroids. The majority of the studies with MCTSs have focused on the role of the mitochondrial

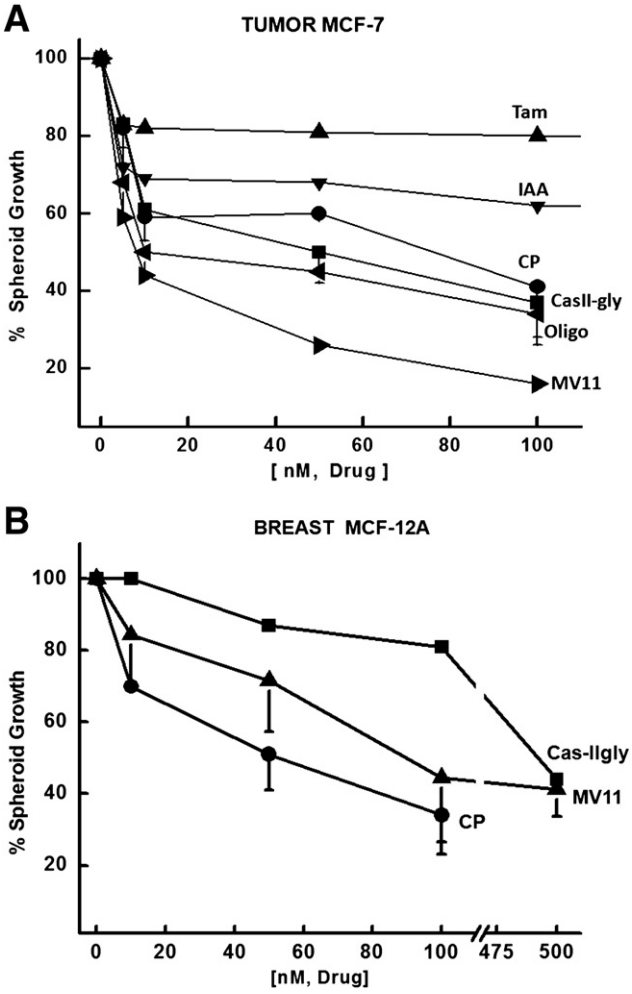

Fig. 4. Effect of oxidative and glycolytic inhibitors, and canonic chemotherapy drugs on MCF-7 (A) and MCF12A (B) spheroid growth. Spheroids were grown as described under Materials and methods. All inhibitors or drugs used were added at the beginning of the spheroid formation (day 5). Spheroid growth values were normalized *vs.* non-inhibited growth at day 17 (MCF-7 MCTS diameter ≈760 nm) or at day 11 (MCF12A spheroid diameter ≈360 nm). Abbreviations: CasII-gly, Casiopeina II-gly; CP, cisplatin; IAA, iodoacetate; MV11, Mitoves; Tam, tamoxifen, Oligo, oligomycin. Data shown represent the mean ± SD of 3 independent preparations except for MCF12 A + Cas-IIgly (n = 2).

Table 2
IC_{50} (nM) values of metabolic and canonical anticancer drugs in non-tumor and tumor spheroids.

Drugs	MCF-7 spheroids		MCF12A spheroids
	Initial cluster	Well-formed	Initial cluster
Anti-mitochondrial			
MV11	7 ± 1.6 (3)	9.7 ± 3 (3)	96 ± 14 (3)
CasII-gly	40 ± 14 (3)	28 (2)	360 (2)
Rhod123	> 500 (3)		
Rhod 6G	79 ± 18 (3)		
Oligo	11 ± 4 (3)		
Anti-glycolytic			
IAA	> 500 (3)		
Canonical			
Tam	> 500 (3)		
CP	76 ± 1.3 (3)	55 ± 5 (3)	54 ± 20 (3)

The indicated drugs were added at the beginning of the spheroid formation (day 5 for both spheroids, *initial cluster*) and the IC_{50} values were determined at day 17 (MCF-7, diameter ≈760 μm), or at day 11 for non-tumor spheroids (MCF-12A, diameter ≈360 μm). The drugs were also added to *well-formed* tumor spheroids (at day 15 of culture, diameter ≈500 μm).

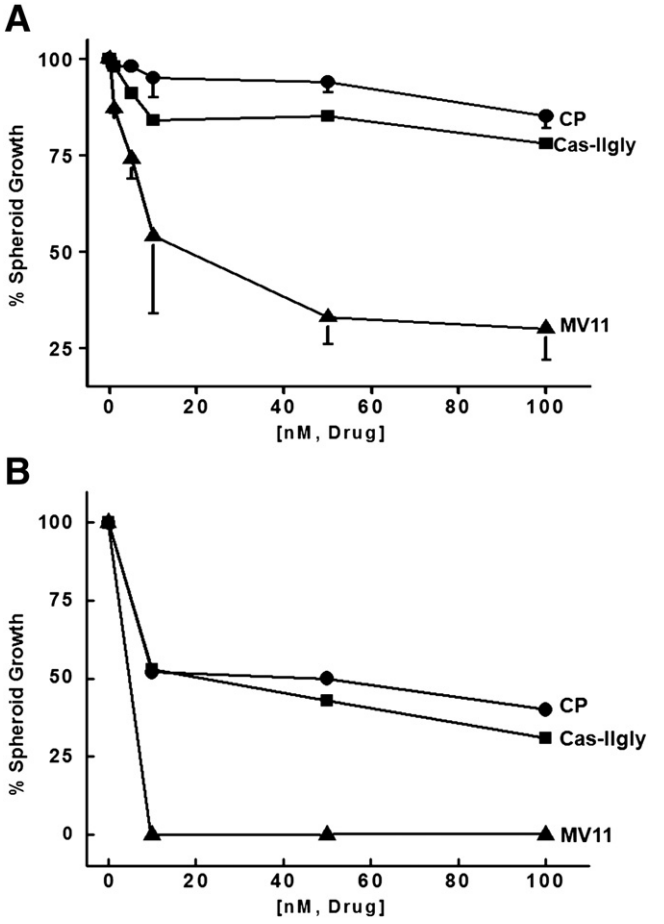

Fig. 5. Effect of Cas-IIgly, MV11 and CP on mature MCF-7 MCTS. All drugs were added at day 15 once MCTSs reached around 500 μM of diameter. MCF-7 MCTSs were recollected at day 18 (A) or day 21(B) after drug addition. Abbreviations are as in Fig. 4. Data shown represent the mean ± SD of 3 independent experiments except for Cas-IIgly (n = 2).

function [16,22,61]. In this regard, it has been documented that the mitochondrial density and total oxygen consumption are similar across the rim of human melanoma MCTSs [61]. However, total cellular respiration does not accurately reflect mitochondrial ATP synthesis because high activities of non-mitochondrial O_2-consumption enzymes (hemo oxygenases, cytochrome p450 and NADPH oxidase) are also developed in tumor spheroid models [25,26]. Therefore, oligomycin- and cyanide-sensitive cellular respiration should be evaluated for precise determinations of OxPhos and maximal respiratory chain capacity, respectively. For instance, cyanide-sensitive cell respirations of the MCTS PRL and QS layers were 73 and 52%, respectively, of the total cell respirations (see values in the legend to Table 1), indicating significant O_2 consumption by non-mitochondrial processes and perhaps production of radical oxygen species by the respiratory chain.

Nonetheless, in dissected rodent EMT6 and 9L MCTSs a severe diminution (60%) in total oxygen consumption on quiescent *vs.* external cellular fraction has been described [16,22], which is of a very similar extent (61%) to that determined in the present study for cyanide-sensitive respiration in MCF-7 MCTS QS cell layers *versus* PRL layers (Table 1). Moreover, in EMT6 and 9L MCTS cellular populations located close to hypoxic and hypoglucemic areas, a drastic mitochondrial protein down-regulation (1–9 times, except for ANT) has also been reported, which was also observed for the contents of mitochondrial proteins of MCF-7 MCTS QS layers (except for SDH and ANT; Fig. 2B) and HeLa cells cultured in monolayers under severe and prolonged hypoxia (0.1% O_2 for 24 h) [28].

OxPhos flux values in both QS and PRL cellular populations were 3–7 times higher than their monolayer (*cf.* Table 1) counterparts and than other bi-dimensional cultured tumor cells (HepG2), which indicates that the spheroid tri-dimensional arrangement (*i.e.*, metabolite gradients and differential transcription factors and oncogene expression profiles) somehow favors oxidative metabolism independently of nutrient and O_2 supply [58]. Cyanide-sensitive and oligomycin-insensitive respiration was also higher (11–29% of total respiration) in both MCF-7 MCTS cell layers than that reported for MCF-7 monolayers (10–15% of total respiration), suggesting an increased passive H^+ diffusion across the inner mitochondrial membrane probably derived from higher contents of uncoupling proteins as described for human colon adenocarcinoma [25,26,62].

4.2. Similar glycolytic metabolism in quiescent- and proliferative-enriched MCF-7 MCTS layers

The hypoxic microenvironment generated in the center of mature MCTSs formed from MCF-7 and other tumor cell lines [51,63] or the exposure of tumor cell monolayers to severe and prolonged hypoxia [28] induces the up-regulation of glycolytic enzymes, activities and fluxes. Stabilization of HIF-1α is involved in the solid tumor adaptation to the hypoxic microenvironment (Figs. 2A, 3A) [64,65, reviewed in 10], particularly of the QS cell fraction (Fig. 1B).

However, in the MCTS PRL-enriched cell fraction, where O_2 availability is high, HIF-1α stabilization is also observed as well as the significant increase (4–5 times) in HIF-1α glycolytic target gene expression, enzyme activities (especially HK, one of the main controlling sites of tumor glycolysis [36]), and pathway flux (Fig. 2A, Table 1), compared with MCF-7 monolayer cells [28]. Similar results have also been described for tumor spheroids from human glioma BMG-1 and transformed rat embryo fibroblast Rat1-T1, in which glycolysis increased 1.5–2.5 times *versus* monolayer counterparts [60,66]. Thus, the present results with the MCTS PRL cell layers suggest that HIF-1α stabilization may also be triggered by (i) accumulation of relevant metabolites such as pyruvate/lactate and succinate/fumarate, which compete with the prolyl hydroxylases substrate 2-OG, thus avoiding HIF-1α degradation; and/or (ii) activation through p53, h-Ras or PTEN oncogenes [67, reviewed in 10] as observed in prostate tumor cells [68].

4.3. Underlying mechanism of OxPhos enhancement in MCF-7 MCTS enriched proliferative cellular populations

Recently, it has been demonstrated that numerous transcription factors such as p32, h-Ras, c-Myc, and PGC-1α positively modulate OxPhos in well-oxygenated areas. p32 and h-Ras participate in the activation of the *novo* synthesis of tumor respiratory chain components such as respiratory complex I, cytochrome *c* oxidase, ATP synthase and pyruvate dehydrogenase [46,47], whereas PGC-1α is associated with the activation of the free fatty acid mitochondrial β-oxidation [reviewed in 48]. Also, PGC-1α and c-Myc have been associated with activation of mitochondrial biogenesis under normoxic conditions [69, reviewed in 48] and glutaminase-K expression in tumor cells (pancreatic cancer PANC-1 and MIA PaCa-2, breast cancer MDA-MB-453) that are close to blood vessel regions [69].

In the PRL cell fraction which is exposed to high oxygen concentrations [28], all these transcription factors were found 2–9 times increased compared to the QS-enriched cell fraction (Fig. 3A), therefore indicating a more active mitochondrial metabolism that correlated with increased (3–7 times) levels of the ATP synthase, COX-IV, PDH-E1α and complex I subunit 1, and OxPhos flux (2-times). The high contents of c-Myc, h-Ras and p32 found in the PRL layer were similar to those found in bi-dimensional cultured under normoxic conditions (Fig. 3A), indicating that factors different from hypoxia and the tri-dimensional architecture may induce their cellular synthesis and stabilization. On the contrary, the levels of p32 and h-Ras in the QS fraction were lower than those determined in MCF-7 cultured in monolayer under hypoxic conditions; whereas PGC-1α was not detected in normoxic monolayer cells, suggesting that the tri-dimensional array may favor their *de novo* synthesis and stabilization.

Several mechanisms have been proposed to explain the low mitochondrial functionality in tumor quiescent cells. Freyer [16,22] proposed that the decrease in mitochondrial oxidative metabolism was associated with a significant diminution in the actin content and consequently low cellular volume, as occurs in prostate MCTS [70]. Another mechanism could be the increase in reactive oxygen species. In this regard, it has been shown a significant ROS accumulation in the inner layers of mature glioma spheroids [reviewed in 71] which affects mitochondrial functionality through mitophagy activation.

In hepatocellular tumor cells, moderate hypoxia (8 h, 1% O_2) activates organelle degradation (peroxisomes, endoplasmic reticulum, ribosomes and principally mitochondria) as a survival mechanism maintaining nutrient supply [72,73]. In order to determine whether mitophagy activation [74,75] was involved in the observed lower mitochondrial function in the QS layers, a panel of essential mitophagy proteins was determined in the MCTS cell fractions. Elevated contents (3–5 times) of Atg7 (required for peroxisomal and vacuolar membranes fusion), Beclin (required for autophagy onset and autophagosome formation), LAMP (required for lysosome biogenesis) and Bnip3 (potent autophagy inducer) were detected in the QS fraction *versus* PRL fraction, suggesting that MCTS QS cells were actively engaged in mitochondrial degradation by lysosomal digestion (Fig. 3B). Except for Atg7, the contents of the mitophagy proteins were similar between MCTS QS layers and hypoxic monolayer cells (*cf.* Fig. 3B) indicating that indeed, hypoxia could be the main inducer of mitophagy protein synthesis.

The present study clearly demonstrates that both dissociated PRL and QS layers maintain high dependency on OxPhos (*cf.* Table 1), which contrasts with the entire and mature tumor spheroids where the cellular ATP required for tumor growth is principally supplied by glycolysis [7]. In the entire spheroids, three tumor microregions (proliferative, quiescent and necro-apoptotic areas) co-exist providing their well-defined 3D structure [11]. Specially, the apoptotic area concentrates, and very likely produces high lactate content [65], which may contribute to the high glycolysis rate found in the entire spheroids. After spheroid dissociation (*cf.* Table 1, Fig. 2) the apoptotic area is totally removed, the extra-lactate is eliminated and in consequence, no over-estimated lactate production is attained for the QS cell layers.

4.4. Anti-mitochondrial therapy as a potential anticancer strategy against breast cancer

The identification of OxPhos as the main pathway for ATP supply in each tri-dimensional tumor cellular layer provides the rational basis for the use of mitochondrial inhibitors to selectively arrest tumor proliferation. Indeed, the specific ATP synthase inhibitor oligomycin, as well as the energy metabolism inhibitors CasII-gly [reviewed in 51] and Mitoves [54] but not rhodamines 123 or 6G, potently and selectively inhibited the growth of breast tumor MCF-7 MCTSs (Fig. 4A) and induced cell death in well-formed MCTSs (Fig. 5) [51]. Rhodamines 123 and 6G as well as Cas-IIgly and Mitoves are lipophilic cations which are expected to accumulate into functional mitochondria in a process driven by the H^+ electrochemical gradient (inside negative) generated by the respiratory chain [reviewed in 51]. However, the lower rhodamine potency to abolish tumor growth suggests that the positive charge and the lipophilic nature targeting mitochondria do not suffice to efficiently stop cancer cell growth. Cas-IIgy and Mitoves have additional features for their specific OxPhos targeting: Cas-IIgly is also a SH-group reagent that more specifically targets 2-OGDH, PDH and SDH [reviewed in 51]; Mitoves acts as an uncoupler and also targets

respiratory complex II [54]. Apparently, these other characteristics augment their antitumor potency.

Interestingly, the same doses of either anti-mitochondrial drug did not affect the growth of non-tumor cells (Fig. 4B) suggesting that OxPhos and mitochondria targeted by highly selective drugs such as Cas IIgly or MV11 may be an effective therapeutic strategy against breast cancer. Moreover, the anticancer activity of the mitochondrial inhibitors, when added either at the beginning of the MCTS growth or during growth of well-formed MCTS indicates that these drugs may prevent and revert tumor cell proliferation.

Platinum-based chemotherapy (CP) and the positive estrogen receptor (ER+) blockers (tamoxifen, Tam) are routinely used in the clinical treatment of early stage and positive ER breast cancer [76,77]. However, growth of MCF-7 MCTS, which represents an ER positive breast carcinoma [78] was only slightly affected by Tam at 100 nM (Figs. 4A and 5). In fact, it has been demonstrated that micromolar doses of Tam are required to block MCF-7 cellular cycle and other processes associated with tumor apoptosis onset [79,80]. However, Tam micromolar doses may prompt unspecific side-effects affecting non-tumor cells in the host such as erythrocytes [81]. Growth of MCF-7 MCTSs was also highly sensitive to CP. Platinum-based drugs destabilize DNA forming adducts, although at doses at which tumor growth is arrested, these drugs also diminish respiratory chain complexes I, III and IV activities and induce collapse of the mitochondrial membrane potential [reviewed in 51,82,83]. Then, unspecific effects of CP are expected on non-tumor cells as shown here for non-tumor MCTS growth (Fig. 4B).

5. Concluding remarks

The analysis of the bioenergetics of the two cellular populations constituting MCTSs, a solid tumor-like model revealed that (i) OxPhos was the predominant pathway for energy supply in both PRL and QS cells and (ii) there appears to be an interrelationship between oncogenes (h-Ras, c-Myc) and tumor transcription factors (p32, PGC-1α) with the contents of autophagy and mitochondrial energy metabolism proteins. These observations suggest that using anti-mitochondrial drugs (*i.e.*, lipophilic cations) such as rhodamines, vitamin E analogs, and copper-based compounds [reviewed in 84] to develop alternative cancer treatment therapies may become promising strategies against fast-growing breast tumors. This proposal was supported by the observed potent and selective effect of these drugs on MCTS growth. Furthermore, as glycolysis is involved in the ATP supply as well as in the supply of essential metabolites required for biosynthetic pathways (nucleotides, triacylglycerides and phospholipids, and some amino acids), a multiple site therapy against energy metabolism (epitomized by Cas-IIgly, which blocks both OxPhos and glycolysis) [85] emerges as a suitable alternative strategy to efficiently arrest solid tumor growth [86,87].

Acknowledgements

The present work was partially supported by grants 80534, 107183, 123636 and 180322 from CONACyT-México and PICS08-5 from the Instituto de Ciencia y Tecnología del Distrito Federal. EAMT was supported by a CONACyT-México fellowship (No. 269132).

References

[1] R. Moreno-Sánchez, S. Rodríguez-Enríquez, A. Marín-Hernández, E. Saavedra, Energy metabolism in tumor cells, FEBS J. 274 (2007) 1393–1418.
[2] S.P. Mathupala, Y.H. Ko, P.L. Pedersen, The pivotal roles of mitochondria in cancer: Warburg and beyond and encouraging prospects for effective therapies, Biochim. Biophys. Acta 1797 (2010) 1225–1230.
[3] X.L. Zu, M. Guppy, Cancer metabolism: facts, fantasy, and fiction, Biochem. Biophys. Res. Commun. 313 (2004) 459–465.
[4] S. Rodríguez-Enríquez, P.A. Vital-Gonzáles, F.L. Flores-Enríquez, A. Marín-Hernández, L. Ruiz-Azuara, R. Moreno-Sánchez, Control of cellular proliferation by modulation of oxidative phosphorylation in human and rodent fast-growing tumor cells, Toxicol. Appl. Pharmacol. 215 (2006) 208–217.
[5] W. Mueller-Klieser, Three-dimensional cell cultures: from molecular mechanisms to clinical applications, Am. J. Physiol. 273 (1997) 1109–1123.
[6] L.A. Kunz-Schughart, Multicellular tumor spheroids: intermediates between monolayer culture and in vivo tumor, Cell Biol. Int. 23 (1999) 157–161.
[7] S. Rodríguez-Enríquez, J.C. Gallardo-Pérez, A. Avilés-Salas, A. Marín-Hernández, L. Carreño-Fuentes, V. Maldonado-Lagunas, R. Moreno-Sánchez, Energy metabolism transition in multi-cellular human tumor spheroids, J. Cell. Physiol. 216 (2008) 189–197.
[8] C. Menon, G.M. Polin, I. Prabakaran, A. His, C. Cheung, J.P. Culver, J.F. Pingpank, C.S. Sehgal, A.G. Yodh, D.G. Buerk, D.L. Fraker, An integrated approach to measuring tumor oxygen status using human melanoma xenografts as a model, Cancer Res. 63 (2003) 7232–7240.
[9] A. Yaromina, S. Meyer, C. Fabian, K. Zaleska, U.G. Sattler, L.A. Kunz-Schughart, W. Mueller-Klieser, D. Zips, M. Baumann, Effects of three modifiers of glycolysis on ATP, lactate, hypoxia, and growth in human tumor cell lines in vivo, Strahlenther. Onkol. 188 (2012) 431–437.
[10] A. Marín-Hernández, J.C. Gallardo-Pérez, S.J. Ralph, S. Rodríguez-Enríquez, R. Moreno-Sánchez, HIF-1alpha modulates energy metabolism in cancer cells by inducing over-expression of specific glycolytic isoforms, Mini Rev. Med. Chem. 9 (2009) 1084–1101.
[11] R. Sutherland, J. Freyer, W. Mueller-Klieser, R. Wilson, C. Heacock, J. Sciandra, B. Sordat, Cellular growth and metabolic adaptations to nutrient stress environments in tumor microregions, Int. J. Radiat. Oncol. Biol. Phys. 12 (1986) 611–615.
[12] J.P. Freyer, P.L. Schor, Regrowth kinetics of cells from different regions of multicellular spheroids of four cell lines, J. Cell. Physiol. 138 (1989) 384–392.
[13] J.P. Freyer, R.M. Sutherland, Selective dissociation and characterization of cells from different regions of multicell tumor spheroids, Cancer Res. 40 (1980) 3956–3965.
[14] C.K. Luk, P.C. Keng, R.M. Sutherland, Radiation response of proliferating and quiescent subpopulations isolated from multicellular spheroids, Br. J. Cancer 54 (1986) 25–32.
[15] C. Gronvik, J. Capala, J. Carlsson, The non-variation in radiosensitivity of different proliferative states of human glioma cells, Anticancer Res. 16 (1996) 25–31.
[16] J.P. Freyer, Decreased mitochondrial function in quiescent cells isolated from multicellular tumor spheroids, J. Cell. Physiol. 176 (1998) 138–149.
[17] L.A. Kunz-Schughart, M. Kreutz, R. Knuechel, Multicellular spheroids: a three-dimensional in vitro culture system to study tumour biology, Int. J. Exp. Pathol. 79 (1998) 1–23.
[18] M.J. Tindall, C.P. Please, Modelling the cell cycle and cell movement in multicellular tumour spheroids, Bull. Math. Biol. 69 (2007) 1147–1165.
[19] J.A. Engelberg, G.E. Ropella, C.A. Hunt, Essential operating principles for tumor spheroid growth, BMC Syst. Biol. 2 (2008) 110.
[20] O.F. Qvarnstrom, M. Simonsson, V. Eriksson, I. Turesson, J. Carlsson, Gamma H2AX and cleaved PARP-1 as apoptotic markers in irradiated breast cancer BT474 cellular spheroids, Int. J. Oncol. 35 (2009) 41–47.
[21] F. Hirschhaeuser, H. Menne, C. Dittfeld, J. West, W. Mueller-Klieser, L.A. Kunz-Schughart, Multicellular tumor spheroids: an underestimated tool is catching up again, J. Biotechnol. 148 (2010) 3–15.
[22] J.P. Freyer, Rates of oxygen consumption for proliferating and quiescent cells isolated from multicellular tumor spheroids, Adv. Exp. Med. Biol. 345 (1994) 335–342.
[23] R.K. Emaus, R. Grunwald, J.J. Lemasters, Rhodamine 123 as a probe of transmembrane potential in isolated rat-liver mitochondria: spectral and metabolic properties, Biochim. Biophys. Acta 850 (1986) 436–448.
[24] S. Ranganathan, R.D. Hood, Effects of in vivo and in vitro exposure to rhodamine dyes on mitochondrial function of mouse embryos, Teratog. Carcinog. Mutagen. 9 (1989) 29–37.
[25] B.J. Murphy, K.R. Laderoute, H.J. Vreman, T.D. Grant, N.S. Gill, D.K. Stevenson, R.M. Sutherland, Enhancement of heme oxygenase expression and activity in A431 squamous carcinoma multicellular tumor spheroids, Cancer Res. 53 (1993) 2700–2703.
[26] F.J. Wu, J.R. Friend, R.P. Remmel, F.B. Cerra, W.S. Hu, Enhanced cytochrome P450 IA1 activity of self-assembled rat hepatocyte spheroids, Cell Transplant. 8 (1999) 233–246.
[27] P. Sonveaux, F. Végran, T. Schroeder, M.C. Wergin, J. Verrax, Z.N. Rabbani, C.J. De saedeleer, K.M. Kennedy, C. Diepart, B.F. Jordan, M.J. Kelley, B. Gallez, M.L. Wahl, O. Feron, M.W. Dewhirst, Targeting lactate-fueled respiration selectively kills hypoxic tumor cells in mice, J. Clin. Invest. 118 (2008) 3930–3942.
[28] S. Rodríguez-Enríquez, L. Carreño-Fuentes, J.C. Gallardo-Pérez, E. Saavedra, H. Quezada, A. Vega, A. Marín-Hernández, V. Olín-Sandoval, M.E. Torres-Márquez, R. Moreno Sánchez, Oxidative phosphorylation is impaired by prolonged hypoxia in breast and possibly in cervix carcinoma, Int. J. Biochem. Cell Biol. 42 (2010) 1744–1751.
[29] J.M. Yuhas, A.P. Li, A.O. Martinez, A.J. Ladman, A simplified method for production and growth of multicellular tumor spheroids, Cancer Res. 37 (1977) 3639–3643.
[30] J. Carlsson, J.M. Yuhas, Liquid-overlay culture of cellular spheroids, Cancer Res. 95 (1984) 1–23.
[31] S. García, J.P. Dales, J. Jacquemier, E. Charafe-Jauffret, D. Birnbaum, L. Andrac-Meyers, M.N. Lavaut, C. Allasia, S. Carpentier-Meunier, P. Bonnier, C. Charpin-Taranger, c-Met overexpression in inflammatory breast carcinoma: automated quantification on tissue microarrays, Br. J. Cancer 96 (2007) 329–335.
[32] H.U. Bergmeyer, E. Bernt, Methods of Enzymatic Analysis, Second ed. Orlando, FL, 1974.

[33] H.U. Bergmeyer, Methods of Enzymatic Analysis, Third ed. Weinheim, Germany, 1984.
[34] S. Ferguson-Miller, D.L. Brautigan, E. Margoliash, Correlation of the kinetics of electron transfer activity of various eukaryotic cytochromes c with binding to mitochondrial cytochrome c oxidase, J. Biol. Chem. 251 (1976) 1104–1115.
[35] J.M. Armstrong, The molar extinction coefficient of 2,6-dichlorophenol indophenols, Biochim. Biophys. Acta 86 (1964) 194–197.
[36] A. Marín-Hernández, S. Rodríguez-Enríquez, P.A. Vital-González, F.L. Flores-Rodríguez, M. Macías-Silva, M. Sosa-Garrocho, R. Moreno-Sánchez, Determining and understanding the control of glycolysis in fast-growth tumor cells. Flux control by an over-expressed but strongly product-inhibited hexokinase, FEBS J. 273 (2006) 1975–1988.
[37] G.D. Bowman, M. O'Donnell, J. Kuriyan, Structural analysis of a eukaryotic sliding DNA clamp-clamp loader complex, Nature 429 (2004) 724–730.
[38] J. Massague, G1 cell-cycle control and cancer, Nature 432 (2004) 298–306.
[39] M.L. Macheda, S. Rogers, J.D. Best, Molecular and cellular regulation of glucose transporter (GLUT) proteins in cancer, J. Cell. Physiol. 202 (2005) 654–662.
[40] I.F. Robey, A.D. Lien, S.J. Welsh, B.K. Baggett, R.J. Gillies, Hypoxia-inducible factor-1alpha and the glycolytic phenotype in tumors, Neoplasia 7 (2005) 324–330.
[41] G.L. Semenza, HIF-1: upstream and downstream of cancer metabolism, Curr. Opin. Genet. Dev. 20 (2010) 51–56.
[42] S. Mazurek, A. Michel, E. Eigenbrodt, Effect of extracellular AMP on cell proliferation and metabolism of breast cancer cell lines with high and low glycolytic rates, J. Biol. Chem. 272 (1997) 4941–4952.
[43] R.A. Nakashima, M.G. Paggi, L.J. Scott, P.L. Pedersen, Purification and characterization of a bindable form of mitochondrial bound hexokinase from the highly glycolytic AS-30D rat hepatoma cell line, Cancer Res. 48 (1988) 913–919.
[44] M.A. dos Santos, J.B. Borges, D.C. de Almeida, R. Curi, Metabolism of the microregions of human breast cancer, Cancer Lett. 216 (2004) 243–248.
[45] S. Simaga, M. Osmak, D. Babic, M. Sprem, B. Vukelic, M. Abramic, Quantitative biochemical analysis of lactate dehydrogenase in human ovarian tissues: correlation with tumor grade, Int. J. Gynecol. Cancer 15 (2005) 438–444.
[46] S. Telang, A.N. Lane, K.K. Nelson, S. Arumugam, J. Chesney, The oncoprotein H-RasV12 increases mitochondrial metabolism, Mol. Cancer 6 (2007) 77.
[47] V. Fogal, A.D. Richardson, P.P. Karmali, I.E. Scheffler, J.W. Smith, E. Ruoslahti, Mitochondrial p32 protein is a critical regulator of tumor metabolism via maintenance of oxidative phosphorylation, Mol. Cell. Biol. 30 (2010) 1303–1318.
[48] E.H. Jeninga, K. Schoonjans, J. Auwerx, Reversible acetylation of PGC-1: connecting energy sensors and effectors to guarantee metabolic flexibility, Oncogene 29 (2010) 4617–4624.
[49] C. Jose, N. Bellance, R. Rossignol, Choosing between glycolysis and oxidative phosphorylation: a tumor's dilemma? Biochim. Biophys. Acta 1807 (2011) 552–561.
[50] A.R. Salomon, D.W. Voehringer, L.A. Herzenberg, C. Khosla, Understanding and exploiting the mechanistic basis for selectivity of polyketide inhibitors of F(0) F(1)-ATPase, Proc. Natl. Acad. Sci. U. S. A. 97 (2000) 14766–14771.
[51] S. Rodríguez-Enríquez, A. Marín-Hernández, J.C. Gallardo-Pérez, L. Carreño-Fuentes, R. Moreno-Sánchez, Targeting of cancer energy metabolism, Mol. Nutr. Food Res. 53 (2009) 29–48.
[52] R. Kramar, M. Hohenegger, A.N. Srour, G. Khanakah, Oligomycin toxicity in intact rats, Agents Actions 15 (1984) 660–663.
[53] C. Hilliard, R. Hill, M. Armstrong, C. Fleckenstein, J. Crowley, E. Freeland, D. Duffy, S.M. Galloway, Chromosome aberrations in Chinese hamster and human cells: a comparison using compounds with various genotoxicity profiles, Mutat. Res. 616 (2007) 103–118.
[54] S. Rodríguez-Enríquez, L. Hernández-Esquivel, A. Marín-Hernández, L.F. Dong, E.T. Akporiaye, J. Neuzil, S.J. Ralph, R. Moreno-Sánchez, Molecular mechanism for the selective impairment of cancer mitochondrial function by a mitochondrially targeted vitamin E analogue, Biochim. Biophys. Acta 1817 (2012) 1597–1607.
[55] J.A. Smith, H. Ngo, M.C. Martin, J.K. Wolf, An evaluation of cytotoxicity of the taxane and platinum agents combination treatment in a panel of human ovarian carcinoma cell lines, Gynecol. Oncol. 98 (2005) 141–145.
[56] P.M. Chu, S.H. Chiou, T.L. Su, Y.J. Lee, L.H. Chen, Y.W. Chen, S.H. Yen, M.T. Chen, M.H. Chen, Y.H. Shih, P.H. Tu, H.I. Ma, Enhancement of radiosensitivity in human glioblastoma cells by the DNA N-mustard alkylating agent BO-1051 through augmented and sustained DNA damage response, Radiat. Oncol. 6 (2011) 7.
[57] W. Mueller-Klieser, Multicellular spheroids. A review on cellular aggregates in cancer research, J. Cancer Res. Clin. Oncol. 113 (1987) 101–122.
[58] L.A. Kunz-Schughart, J. Doetsch, W. Mueller-Klieser, K. Groebe, Proliferative activity and tumorigenic conversion: impact on cellular metabolism in 3-D culture, Am. J. Physiol. Cell Physiol. 278 (2000) C765–780.
[59] K. Weber, D. Ridderskamp, M. Alfert, S. Hoyer, R.J. Wiesner, Cultivation in glucose-deprived medium stimulates mitochondrial biogenesis and oxidative metabolism in HepG2 hepatoma cells, Biol. Chem. 383 (2002) 283–290.
[60] D. Khaitan, S. Chandna, M.B. Arya, B.S. Dwarakanath, Differential mechanisms of radiosensitization by 2-deoxy-D-glucose in the monolayers and multicellular spheroids of a human glioma cell line, Cancer Biol. Ther. 5 (2006) 1142–1151.
[61] M.E. Hystad, E.K. Rofstad, Oxygen consumption rate and mitochondrial density in human melanoma monolayer cultures and multicellular spheroids, Int. J. Cancer 57 (1994) 532–537.
[62] M. Horimoto, M.B. Resnick, T.A. Konkin, J. Routhier, J.R. Wands, G. Baffy, Expression of uncoupling protein-2 in human colon cancer, Clin. Cancer Res. 10 (2004) 6203–6207.
[63] C. Erlichman, I.F. Tannock, Growth and characterization of multicellular tumor spheroids of human bladder carcinoma origin, In Vitro Cell. Dev. Biol. 22 (1986) 449–456.
[64] N.S. Waleh, M.D. Brody, M.A. Knapp, H.L. Mendoca, E.M. Lord, C.J. Koch, K.R. Laderoute, R.M. Sutherland, Mapping of the vascular endothelial growth factor-producing hypoxic cells in multicellular tumor spheroids using a hypoxia-specific marker, Cancer Res. 55 (1995) 6222–6226.
[65] R.A. Gatenby, R.J. Gillies, Why do cancers have high aerobic glycolysis? Nat. Rev. Cancer 4 (2004) 891–899.
[66] S. Walenta, J. Doetsch, W. Mueller-Klieser, L.A. Kunz-Schughart, Metabolic imaging in multicellular spheroids of oncogene-transfected fibroblasts, J. Histochem. Cytochem. 48 (2000) 509–522.
[67] H. Lu, C.L. Dalgard, A. Mohyeldin, T. McFate, A.S. Tait, A. Verma, Reversible inactivation of HIF-1 prolyl hydroxylases allows cell metabolism to control basal HIF-1, J. Biol. Chem. 280 (2005) 41928–41939.
[68] A. Mori, C. Moser, S.A. Lang, C. Hackl, E. Gottfried, M. Kreutz, H.J. Sclitt, E.K. Geissler, O. Stoeltzing, Up-regulation of Krüppel-like factor 5 in pancreatic cancer is promoted by interleukin-1beta signaling and hypoxia-inducible factor-1alpha, Mol. Cancer Res. 7 (2009) 1390–1398.
[69] C.V. Dang, A. Le, P. Gao, MYC-induced cancer cell energy metabolism and therapeutic opportunities, Clin. Cancer Res. 15 (2009) 6479–6483.
[70] H. Sauer, J. Ritgen, J. Hescheler, M. Wartenberg, Hypotonic Ca^{2+} signaling and volume regulation in proliferating and quiescent cells from multicellular spheroids, J. Cell. Physiol. 175 (1998) 129–140.
[71] D. Khaitan, B.S. Dwarakanath, Endogenous and induced oxidative stress in multicellular tumour spheroids: implications for improving tumour therapy, Indian J. Biochem. Biophys. 46 (2009) 16–24.
[72] M.M. Hippert, P.S. O'Toole, A. Thorburn, Autophagy in cancer: good, bad, or both? Cancer Res. 66 (2006) 9349–9351.
[73] C.M. Kenific, A. Thorburn, J. Debnath, Autophagy and metastasis: another double-edged sword, Curr. Opin. Cell Biol. 22 (2010) 241–245.
[74] S. Rodríguez-Enríquez, I. Kim, R.T. Currin, J.J. Lemasters, Tracker dyes to probe mitochondrial autophagy (mitophagy) in rat hepatocytes, Autophagy 2 (2006) 39–46.
[75] I. Kim, S. Rodriguez-Enriquez, J.J. Lemasters, Selective degradation of mitochondria by mitophagy, Arch. Biochem. Biophys. 462 (2007) 245–253.
[76] C. Criscitiello, D. Fumagalli, K.S. Saini, S. Loi, Tamoxifen in early-stage estrogen receptor-positive breast cancer: overview of clinical use and molecular biomarkers for patient selection, Onco. Targets Ther. 4 (2010) 1–11.
[77] S.J. Isakoff, Triple-negative breast cancer: role of specific chemotherapy agents, Cancer J. 16 (2010) 53–61.
[78] A.S. Levenson, V.C. Jordan, MCF-7: the first hormone-responsive breast cancer cell line, Cancer Res. 57 (1997) 3071–3078.
[79] R. Perry, Y. Kang, B. Greaves, Effects of tamoxifen on growth and apoptosis of estrogen-dependent and -independent human breast cancer cells, Ann. Surg. Oncol. 2 (1995) 238–245.
[80] A. Otto, R. Paddenberg, S. Schubert, H. Mannhertz, Cell-cycle arrest, micronucleus formation, and cell death in growth inhibition of MCF-7 breast cancer cells by tamoxifen and cisplatin, J. Cancer Res. Clin. Oncol. 22 (1996) 603–612.
[81] I. Afzal, P. Cunningham, R.J. Naftalin, Interactions of ATP, oestradiol, genistein and the anti-oestrogens, faslodex (ICI182780) and tamoxifen, with the human erythrocyte glucose transporter, GLUT1, Biochem. J. 365 (2002) 707–719.
[82] M. Kruidering, B. Van de Water, E. de Heer, G.J. Mulder, J.F. Nagelkerke, Cisplatin-induced nephrotoxicity in porcine proximal tubular cells: mitochondrial dysfunction by inhibition of complexes I to IV of the respiratory chain, J. Pharmacol. Exp. Ther. 280 (1997) 638–649.
[83] M. Montopoli, M. Bellanda, F. Lonardoni, E. Ragazzi, P. Dorigo, G. Froldi, S. Mammi, L. Caparrotta, "Metabolic reprogramming" in ovarian cancer cells resistant to cisplatin, Curr. Cancer Drug Targets 11 (2011) 226–235.
[84] S. Rodríguez-Enríquez, J.C. Gallardo-Pérez, A. Marín-Hernández, J.L. Aguilar-Ponce, E.A. Mandujano-Tinoco, A. Meneses, R. Moreno-Sánchez, Oxidative phosphorylation as a target to arrest malignant neoplasias, Curr. Med. Chem. 18 (2011) 3156–3167.
[85] A. Marín-Hernández, J.C. Gallardo-Pérez, S.Y. López-Ramírez, J.D. García-García, J.S. Rodríguez-Zavala, L. Ruiz-Ramírez, I. Gracia-Mora, A. Zentella-Dehesa, M. Sosa-Garrocho, M. Macías-Silva, R. Moreno-Sánchez, S. Rodríguez-Enríquez, Casiopeina II-gly and bromo-pyruvate inhibition of tumor hexokinase, glycolysis, and oxidative phosphorylation, Arch. Toxicol. 86 (2012) 753–766.
[86] S. Rodríguez-Enríquez, S.C. Pacheco-Velázquez, J.C. Gallardo-Pérez, A. Marín-Hernández, J.L. Aguilar-Ponce, E. Ruíz-García, L.M. Ruizgodoy-Rivera, A. Meneses-García, R. Moreno-Sánchez, Multi-biomarker pattern for tumor identification and prognosis, J. Cell. Biochem. 112 (2011) 2703–2715.
[87] R. Moreno-Sánchez, E. Saavedra, S. Rodríguez-Enríquez, J.C. Gallardo-Pérez, H. Quezada, H.V. Westerhoff, Metabolic control analysis indicates a change of strategy in the treatment of cancer, Mitochondrion 10 (2010) 626–639.
[88] R.A. Nakashima, M.G. Paggi, P.L. Pedersen, Contributions of glycolysis and oxidative phosphorylation to adenosine 5′-triphosphate production in AS-30D hepatoma cells, Cancer Res. 44 (1984) 5702–5706.